Effects of Virion and Salt Concentrations on the Raman Signatures of Filamentous Phages fd, Pf1, Pf3, and PH75†

Stacy A. Overman,‡ David M. Kristensen,‡,§ Priya Bondre,‡ Barbara Hewitt,‡ and George J. Thomas, Jr.*,‡

Division of Cell Biology and Biophysics, School of Biological Sciences, University of Missouri—Kansas City, 5100 Rockhill Road, Kansas City, Missouri 64110

Received July 14, 2004

ABSTRACT: Filamentous phages consist of a single-stranded DNA genome encapsidated by several thousand copies of a small α-helical coat protein subunit plus several copies of four minor proteins at the filament ends. The filamentous phages are important as cloning vectors, vehicles for peptide display, and substrates for macromolecular alignment. Effective use of a filamentous phage in such applications requires an understanding of experimental factors that may influence the propensity of viral filaments to laterally aggregate in solution. Because the Raman spectrum of a filamentous phage is strongly dependent on the relative orientation of the virion with respect to the polarization direction of the electromagnetic radiation employed to excite the spectrum, we have applied Raman spectroscopy to investigate lateral aggregation of phages fd, Pf1, Pf3, and PH75 in solution. The results show that lateral aggregation of the virions and anisotropic orientation of the aggregates are both disfavored by high concentrations of salt (>200 mM NaCl) in solutions containing a relatively low virion concentration (<10 mg/mL). Conversely, the formation of lateral aggregates and their anisotropic orientation are strongly favored by a low salt concentration (<0.1 mM NaCl), irrespective of the virion concentration over a wide range. The use of Raman polarization effects to distinguish isotropic and anisotropic solutions of filamentous phages is consistent with previously reported Raman analyses of virion structures in both solutions and fibers. The Raman data are supported by electron micrographs of negatively stained specimens of phage fd, which permit an independent assessment of salt effects on lateral aggregation. The present results also identify new Raman bands that serve as potential markers of subunit side-chain orientations in filamentous virus assemblies.

Filamentous bacteriophages, which are narrow (∼6 nm width) cylindrical particles ranging in length from ∼0.5 to ∼2 μm depending on strain, are capable of infecting bacteria from greatly diverse environments, including ecosystems of high temperature and high salinity. The typical virion packages a circular and single-stranded (ss)[1] DNA genome of several thousand bases within a capsid comprising several thousand copies of a small and highly α-helical protein (product of viral gene VIII). Several copies of up to four minor proteins also cap the filament ends (*1*, *2*). For the well-characterized phages fd (infecting *Escherichia coli*), Pf1 (*Pseudomonas aeruginosa*, strain K), Pf3 (*P. aeruginosa*, strain PAO), and PH75 (*Thermus thermophilus*), the respective pVIII subunits contain 50, 46, 44, and 46 residues (*2*−*4*). In each case, the capsid subunit has been modeled as a continuous α-helix tilted by a small average angle (16−20°) from the cylindrical axis, such that the acidic N terminus is exposed on the exterior surface of the capsid, the basic C terminus is located along the interior surface, and the intervening residues form a hydrophobic intersubunit interface spanning the 20-Å thick capsid wall (*4*−*10*). Thus, the N and C termini of the capsid subunit are presumed capable of interacting, respectively, with the extraviral medium and the packaged ssDNA genome (*11*). Additional details of filamentous phage architecture and corresponding molecular mechanisms of virion assembly have been probed by genetic (*12*), biochemical (*13*, *14*), and biophysical (*15*−*20*) methods.

Interest in filamentous phage structure and assembly has been fueled by several biologically important roles for the virions. For example, the filamentous phage CTXΦ (*Vibrio cholera*), which carries the gene for cholera toxin, serves as a prime example of horizontal gene transfer (*21*). Phage M13 (*E. coli*), which is virtually identical to fd, serves as an indispensable tool in molecular biology (*22*). Other filamentous phages have been exploited as either vehicles for epitope identification in peptide display (*23*, *24*), models for membrane protein translocation (*25*, *26*), or scaffolds for macromolecular orientation in solution NMR structure determinations (*27*).

Many biophysical applications require unidirectional orientation of the filamentous phage particles in dispersed (solution) or condensed (fiber) states (*2*, *6*, *7*, *28*). The degree of virion orientation, as well as the nature and extent of intra- and intervirion interactions, have long been recognized as

† Part LXXXV in the series Structural Studies of Viruses by Raman Spectroscopy. This work was supported by NIH Grant GM50776.

* To whom correspondence should be addressed. E-mail: thomasgj@umkc.edu. Telephone: 816-235-5247. Fax: 816-235-1503.

‡ University of Missouri—Kansas City.

§ Present address: Structural and Computational Biology and Molecular Biophysics Program, Department of Molecular and Human Genetics, Baylor College of Medicine, One Baylor Plaza, Houston, TX 77030.

[1] Abbreviations: ss, single stranded; NMR, nuclear magnetic resonance; EM, electron microscopy.

10.1021/bi0485023 CCC: $27.50
Published on Web 09/24/2004

sensitive to many environmental factors, including solution or fiber temperature (*9*, *29*), pH (*30*), ionic composition (*31*−*33*), and applied magnetic field strength (*2*, *28*, *34*, *35*). Here, we probe in further detail the effects of two key parameters, solution salt concentration and virion concentration, on the alignment and aggregative properties of phages fd, Pf1, Pf3, and PH75.

The principal technique employed is Raman spectroscopy. The Raman results have been augmented by negative-stain electron microscopy (EM) to permit visualization of oriented virions at conditions comparable to those used for spectroscopic data collections. We interpret the Raman results in terms of phage propensity for lateral intervirion association (clustering) and unidirectional orientation of the clusters. We propose specific experimental conditions that tend to disaggregate clusters of filamentous virions and favor random or isotropic dispersal in solution. These are the conditions best suited for the application of solution Raman spectroscopy (*36*). We also identify experimental conditions that favor clustering of phage particles and nonrandom orientation of the resulting clusters. Such conditions are appropriate for the analysis of oriented fibers or gels by methods of polarized Raman spectroscopy (*37*), X-ray fiber diffraction (*2*), solid-state NMR (*28*), and other techniques (*34*).

The information obtained in this study complements and extends a recent study of metal-ion-induced lateral aggregation of phages fd and M13 (*33*). Importantly, the present Raman results provide a basis for evaluating whether local and/or nonlocal structural perturbations result from lateral interactions of the virions. The process of identification and assignment of orientation-sensitive Raman bands also facilitates their use in the determination of residue geometry in capsid subunits or packaged DNA. Such inferences corroborate vibrational assignments developed previously from detailed Raman studies of isotopically labeled virions (*38*−*41*). Finally, the detection of significant Raman polarization effects in spectra of anisotropically oriented phage clusters identifies vibrational bands that may serve as candidates for future Raman tensor determinations (*37*).

MATERIALS AND METHODS

Growth of Bacteriophage. Mesophilic bacteriophages (fd, Pf1, and Pf3) were grown at 37 °C in enriched media containing the respective host (*E. coli* strain Hfr3300, *P. aeruginosa* strain K, and *P. aeruginosa* strain PAO1 carrying the RP1 plasmid) from laboratory stocks obtained originally from Dr. L. A. Day, Public Health Research Institute. Procedures for harvesting and purifying the virions, which differ for each phage, have been described (*40*, *42*, *43*). Additional information may be found at the laboratory web site (http://sbs.umkc.edu/gjthomas-lab).

The thermophilic bacteriophage PH75 and its host *T. thermophilus* strain HB8 were obtained from Dr. M. R. Slater, Promega Corp., Madison, WI. The phage was grown at 70 °C in accordance with a protocol recommended by Dr. D. M. Pederson, California State University, San Bernardino, CA, in 1 L of medium containing 3 g of tryptone, 3 g of yeast extract, 5 g of disodium succinate, 0.7 g of $NaNO_3$, 0.1 g of $CaCl_2$, 0.1 g of KNO_3, 0.1 g of $MgCl_2$, 2.9 mg of boric acid, 1.8 mg of $MnCl_2$, 0.25 mg of $ZnSO_4$, 0.1 mg of $CuSO_4$, 0.1 mg of $CoCl_3$, and 0.4 mg of Na_2MoO_4. The pH of the medium was adjusted to 8.3 with NaOH. Details for harvesting and purifying PH75 are similar to those used for fd (*40*).

Trizma base buffer, inorganic salts, nutrients, and other ingredients in the growth media were obtained from Sigma (St. Louis, MO) or Fisher Scientific (St. Louis, MO).

Sample Preparations for Raman Spectroscopy. Stock solutions for Raman spectroscopy of each phage (fd, Pf1, Pf3, and PH75) were prepared at four different sets of conditions: (i) low virus (∼10 mg/mL) and high salt (200 mM NaCl) concentrations, (ii) low virus and low salt (no added NaCl) concentrations, (iii) high virus (∼100 mg/mL) and low salt concentrations, and (iv) high virus and high salt concentrations. All solutions also contained 5 mM Tris at pH 7.8. Precise virus concentrations were determined by UV spectroscopy using extinction coefficients of 3.84 mL mg^{-1} cm^{-1} at 269 nm for fd, 2.07 mL mg^{-1} cm^{-1} at 270 nm for Pf1, 4.5 mL mg^{-1} cm^{-1} at 262 nm for Pf3, and 3.77 mL mg^{-1} cm^{-1} at 267 nm for PH75 (*4*, *31*). At the low salt condition, the cation concentration, other than that due to phage and buffer counterions, is presumed insignificant. Although Raman spectra were obtained for the four types of solutions of each phage, we present here only the Raman data collected for conditions (i) and (iii), which favor, respectively, either disaggregation or aggregation of the filamentous particles, as detailed below (see the Discussion and Conclusions section). Spectra obtained at solution conditions (ii) and (iv) are available from the authors upon request.

Raman Spectroscopy. Virus solutions were sealed in glass capillaries (KIMAX number 34507) for Raman analysis. Typically, a 2 μL aliquot was sufficient to fill the portion of the sample cell exposed to laser illumination. Raman spectra were obtained on a Spex 500M single-monochromator spectrograph equipped with a notch filter and charge-coupled device detector (SpectrumOne, Instruments S. A., Edison, NJ). Spectra were excited with 200 mW of the 532 nm line from a solid-state, diode-pumped, frequency-doubled Nd:YVO_4 laser (model Verdi, Coherent, Santa Clara, CA). All spectral data were collected from samples thermostated at 12 °C (*44*). The total acquisition time for each Raman spectrum was either 120 or 30 min for samples containing either a low or high virus concentration, respectively.

Multiple data collections were performed for each sample, at least 10 for fd, Pf1, and Pf3 and at least 3 for PH75 at conditions (i) and (iii). The experiments were also repeated on at least two independently prepared stocks of each of the four viruses. Data obtained from solutions containing low virus concentrations were averaged, baseline corrected, and compensated for buffer contributions using previously described protocols (*45*). Data obtained from solutions containing high virus concentrations generally required no baseline corrections or buffer compensations (*38*, *40*).

Electron Microscopy. Negative-stain electron micrographs were obtained from solutions of the filamentous bacteriophage fd (∼15−18 μg/mL in 10 mM Tris) to observe possible differences in the extent of filament aggregation at different salt and pH conditions. Solutions containing 10 mM Tris, 10 mM Tris plus 50 mM NaCl, and 10 mM Tris plus 500 mM NaCl, each at pH values of 2.0, 7.9, and 11.0, were examined. The virus solutions were applied to carbon-coated copper grids and stained with 2% uranyl acetate. The

negatively stained virus particles were viewed using a 1200 EX II electron microscope (JEOL USA, Inc., Peabody, MA) at 100 kV, and the images were recorded on Kodak Professional Polycontrast III RC paper at 50 000 magnification.

RESULTS AND INTERPRETATION

Concentration Dependence of Raman Spectra. Previous studies have shown that the solution Raman spectrum of a filamentous virus can be impacted significantly by altering the concentration of salt (NaCl) in solutions of fixed virus concentration (*31*). Here, we manipulate the ratio of salt-to-virion by comparing solutions containing low virus and high salt concentrations with solutions containing high virus and low salt concentrations. For convenience, we refer to these two types of solutions as high-salt and low-salt forms, respectively, of the virus. Data are illustrated in Figure 1 for the four filamentous viruses, fd (A), Pf1 (B), Pf3 (C), and PH75 (D). In each case, the low Na^+ solution contains less than 0.1 mM NaCl, i.e., only residual Na^+ remains after the PEG precipitation procedure and the repeated salt-free resuspension protocols noted above (see the Materials and Methods). Accordingly, Na^+ is likely present only as counterions to charged DNA phosphate and subunit carboxylate sites of the virion. Conversely, the high Na^+ condition (200 mM NaCl) corresponds to ~100:1 molar excess of Na^+ per capsid subunit. Figure 1 also shows for each virus the computed Raman difference spectrum in the format low-minus-high salt. The difference signatures are striking for their numerous peaks and troughs, yet no significant Raman wavenumber changes occur. Such difference profiles have been detected previously in polarized Raman analyses of oriented fibers of filamentous viruses (*6*, *10*, *16*, *17*, *46*) and presumably reflect the same phenomenon, namely, a change of average virion orientation in relation to the direction of polarization of the exciting laser radiation without alteration of molecular structure. Table 1 lists the Raman bands of each virus that exhibit the concentration-dependent intensities (Raman polarization effects) and their corresponding assignments. For each virion, the salt-induced intensity perturbations are most significant for amide I (1645−1655 cm^{-1}) and amide III (1270−1310 cm^{-1}) bands of the subunit main chain and for bands of Trp (~757, 1005−1010, ~1205, 1338−1345, 1362, and 1545−1560 cm^{-1}) and Tyr (850−855 and 1605 cm^{-1}) side chains. Raman bands assigned to skeletal C−C stretching modes of nonaromatic side chains (870−1000 and 1050−1200 cm^{-1}) also exhibit polarization effects.

Figure 1 and Table 1 show that the salt-induced perturbations to Raman amide I and amide III intensities are identical in sign and comparable in magnitude (~30−50%) for all viruses. Conversely, different intensity changes are observed for side-chain markers of different viruses. Accordingly, the data imply that in each filamentous virus the subunit main chain is oriented similarly with respect to the virion axis, whereas the side chains are not. The results can be explained by reference to previous polarized Raman studies of oriented fibers of the filamentous viruses (*6*, *10*, *16*, *17*) and by postulating that in the solutions examined here the virions are randomly distributed at high-salt conditions but aligned at low-salt conditions. The nonrandom distribution of virions in a solution containing minimal salt is presumed to result

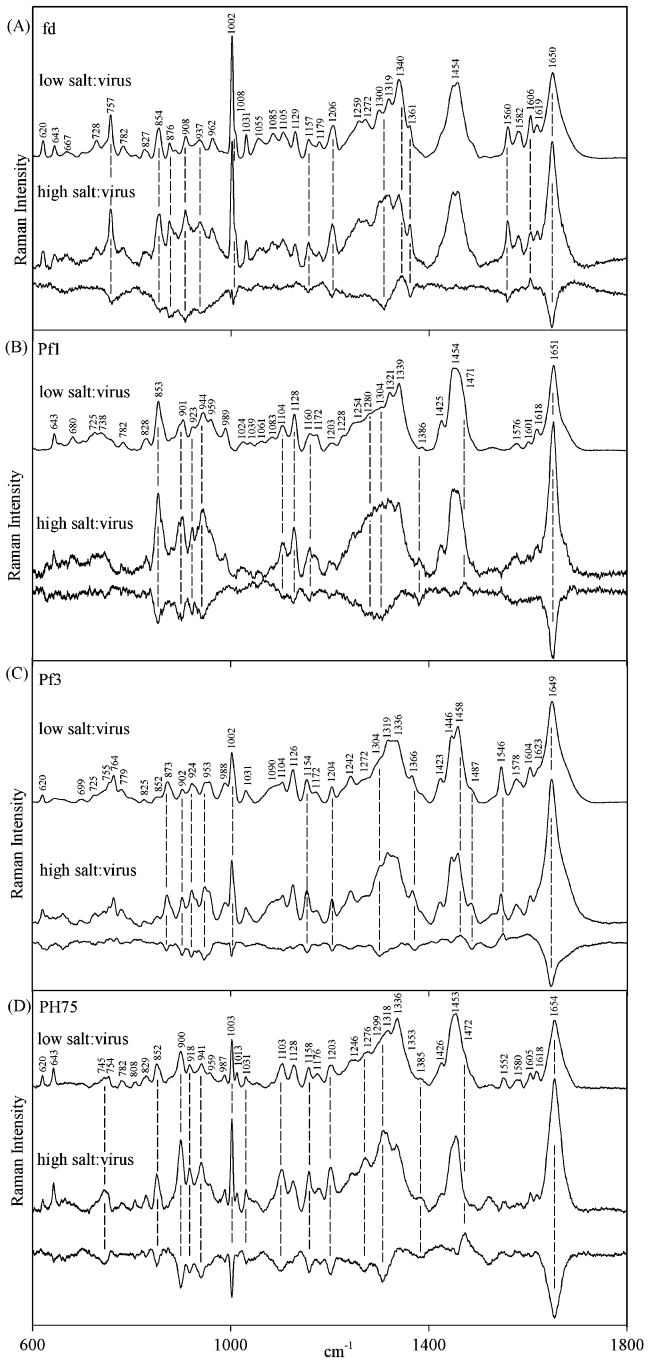

FIGURE 1: Raman spectra (600−1800 cm^{-1}) of four filamentous bacteriophages in solutions of low (top traces) and high (middle traces) salt/virus concentrations and their corresponding differences (bottom traces). Panels (A), (B), (C), and (D) show data for phages fd, Pf1, Pf3, and PH75, respectively. All solutions contain 5 mM Tris at pH 7.8. Low and high salt/virus concentrations correspond, respectively, to ≪0.1 mM NaCl + 100 mg/mL virus and 200 mM NaCl + 10 mg/mL virus.

from extensive intervirion aggregation and preferential alignment of the aggregates within the Raman sample cell. This effectively leads to a liquid crystalline-like phase and a pseudo-polarized Raman signature (top trace in each panel of Figure 1). Conversely, in the virus solutions that contain high salt, the aggregation and alignment of virions are disfavored, leading to a typical isotropic solution Raman spectrum (middle trace in each panel of Figure 1). A schematic representation of this phenomenon is illustrated in Figure 2. The present interpretation is consistent with

Table 1: Raman Bands of Phages fd, Pf1, Pf3, and PH75 Exhibiting Dependence of Intensity on Solution NaCl Concentration

phage	cm^{-1}	I^a	ΔI (%)^b	residue^c	type of mode^d
fd	757	7.8	−27	W	*W18*
	853	7.2	−43	Y, I	*Y1 + 2Y16a*, σ(C−C)
	878	6.5	−62	W, I, V	*W17*, σ(C−C)
	905	7.8	−58	A	$\sigma(C^{\alpha}-C^{\beta}) + \delta$(C−C)
	937	6.2	−56	K, L, V	σ(C−C), $\sigma(C^{\epsilon}-N^{\zeta})$
	1005	16.9	−13	W	*W16*
	1156	3.4	−20	I, V	σ(C−C)
	1203	5.9	−24	F	*F7a*
	1309	9.1	−32	α-helix	amIII
	1345	8.6	+16	W, A, G, K, S, V	*W7′*, $\delta(C^{\alpha}H) + \sigma(C^{\alpha}-C)$, $\delta(CH_2)$, $\delta(C^{\beta}H)$
	1362	5.7	−24	W	*W7″*
	1558	6.2	−33	W	*W3*
	1605	4.7	+22	F, Y	*F8a*, *Y8b*
	1649	16.7	−32	α-helix	amI
Pf1	853	10.1	−37	Y, I	*Y1+2Y16a*, σ(C−C)
	899	6.7	−49	A, K	σ(C−C), $\sigma(C^{\epsilon}-N^{\zeta})$
	921	5.7	−48	V, L	σ(C−C)
	941	8.0	−36	K, L, V	σ(C−C), $\sigma(C^{\epsilon}-N^{\zeta})$
	1106	4.1	−14	A	$\sigma(C^{\alpha}-C^{\beta}) + \delta(C^{\beta}H_3)$
	1126	5.7	−23	I, V, L	σ(C−C)
	1157	3.3	−30	I, V	σ(C−C)
	1281	7.1	−38	α-helix	amIII
	1303	8.3	−34	α-helix	amIII
	1380	2.0	−79	side chains [?]	δ(CH), $\delta(CH_2)$, $\delta(CH_3)$ [?]
	1471	5.1	+19	A, I, L	$\delta(CH_2)$, $\delta(CH_3)$
	1650	18	−44	α-helix	amI
Pf3	870	3.9	−23	W, I, V	*W17*, σ(C−C)
	902	4.1	−43	A	$\sigma(C^{\alpha}-C^{\beta}) + \delta$(C−C)
	920	4.3	−46	V, L	σ(C−C)
	946	5.7	−44	K, L, V	σ(C−C), $\sigma(C^{\epsilon}-N^{\zeta})$
	1004	6.4	−11	W	*W16*
	1154	5.0	−25	I, V	σ(C−C)
	1204	3.8	−29	F	*F7a*
	1300	8.8	−20	α-helix	amIII
	1371	4.5	−24	W	*W7″*
	1459	10.5	+12	I, L, V	$\delta(CH_2)$, $\delta(CH_3)$
	1487	3.0	−29	ade, gua	δ(C2H), σ(N9−C8)
	1549	3.9	+36	W	*W3*
	1647	21.4	−30	α-helix	amI
PH75	759	3.0	−63	W	*W18*
	852	5.1	−44	Y	*Y1 + 2Y16a*
	899	9.7	−52	A	$\sigma(C^{\alpha}-C^{\beta}) + \delta$(C−C)
	917	5.9	−51	V, L	σ(C−C)
	940	6.7	−52	K, L, V	σ(C−C), $\sigma(C^{\epsilon}-N^{\zeta})$
	1003	12.7	−48	F	*F1*
	1031	3.0	−53	F	*F18a*
	1101	5.7	−47	A	$\sigma(C^{\alpha}-C^{\beta}) + \delta(C^{\beta}H_3)$
	1159	5.4	−53	I, V	σ(C−C)
	1201	6.0	−50	F	*F7a*
	1270	7.3	−35	α-helix	amIII
	1307	11.1	−36	α-helix	amIII
	1385	1.9	−40	side chains [?]	δ(CH), $\delta(CH_2)$, $\delta(CH_3)$ [?]
	1472	2.1	+131	A, I, L	$\delta(CH_2)$, $\delta(CH_3)$
	1654	18.3	−47	α-helix	amI

[a] Raman intensity (arbitrary units) is that of the parent band in the phage high-salt spectrum of Figure 1. The Raman wavenumber (cm^{-1} units, column to the left) is that of the difference band from the corresponding phage difference spectrum of Figure 1. [b] Percentage change of Raman intensity between high- and low-salt spectra of Figure 1. [c] Residues, in order of decreasing contribution, to which the Raman band is assigned; one- and three-letter abbreviations are used for coat subunit amino acids and DNA bases, respectively. [d] Abbreviations: σ, bond stretch (atoms in parentheses); δ, bond deformation (group in parentheses); amI, amide I; amIII, amide III; W, tryptophan; Y, tyrosine; F, phenylalanine; normal mode designations for F, W, and Y follow standard notation (reviewed in ref *58*); *W7′* and *W7″* indicate components of Fermi doublets involving *W7*.

previously reported ultraviolet-resonance Raman (UVRR) signatures obtained from solutions of filamentous viruses subjected to a velocity gradient (*7*, *47*). Additional evidence in favor of preferential alignment of filamentous virus aggregates as the salt/virus ratio decreases has been noted by other investigators (*30*, *33*−*35*).

Electron Microscopy. To further support the proposed salt/virus dependence of virion anisotropy and aggregation, we obtained electron micrographs of negatively stained samples of fd over a wide range of salt/virus concentration. Representative data obtained on samples of fd in solutions containing low-, moderate-, and high-salt concentrations are shown in parts A, B, and C, respectively, of Figure 3. The EM images show that the absence of excess NaCl leads to the formation of filament bundles in which the virions are not randomly distributed (A), whereas increasing the con-

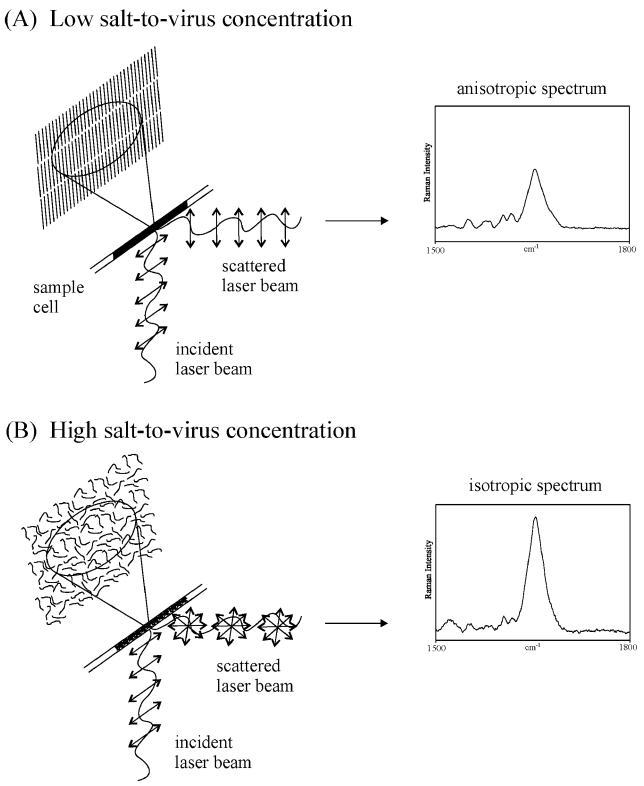

FIGURE 2: Schematic representation of the Raman spectra obtained from (A) anisotropically and (B) isotropically oriented filamentous phages. The spectrum in A is similar to a polarized Raman spectrum obtained from an oriented fiber of the same phage (*6*, *16*, *17*).

centration of NaCl disfavors such aggregation and orientation phenomena (B and C). Similar micrographs were recorded in protocols repeated over a wide range of solution pH (2.0−11.0). The EM images are consistent with the Raman spectra in suggesting that the low salt/virus condition promotes intervirion association and alignment of the resulting filament bundles.

DISCUSSION AND CONCLUSIONS

Effect of Salt on Lateral Association of Filamentous Viruses. Effects of various mono-, di-, and polyvalent cations on the associative properties of filamentous polyelectrolytes have been reviewed recently (*48*). Studies by Tang and coworkers show that in the case of the filamentous viruses fd and M13 several types of orientational and associative phenomena are possible, including (i) partitioning between isotropic and cholesteric phases and (ii) lateral aggregation (bundle formation or clustering), induced by appropriate treatment of an initially isotropic solution of the phage with di- or polyvalent cations (*33*, *49*, *50*). It has also been demonstrated that multivalent cation-induced aggregation of phage fd in solution can be reversed by treatment with the monovalent cation, K^+ (*33*). Similar aggregative phenomena and monovalent cation-induced reversal have also been reported for the filamentous skeletal protein actin (*50*, *51*). Of particular relevance to the interpretation of the current results is the partitioning of fd between isotropic and cholesteric phases, which is dependent not only upon solution ionic strength but also upon phage concentration. On the basis of the earlier studies (*49*), we expect all of the phages examined here to favor isotropy in solutions containing high-salt (200 mM NaCl) and relatively low-virus (∼10 mg/mL) concentrations. Conversely, in the absence of salt and at relatively high-virus concentrations (∼100 mg/mL), cluster-

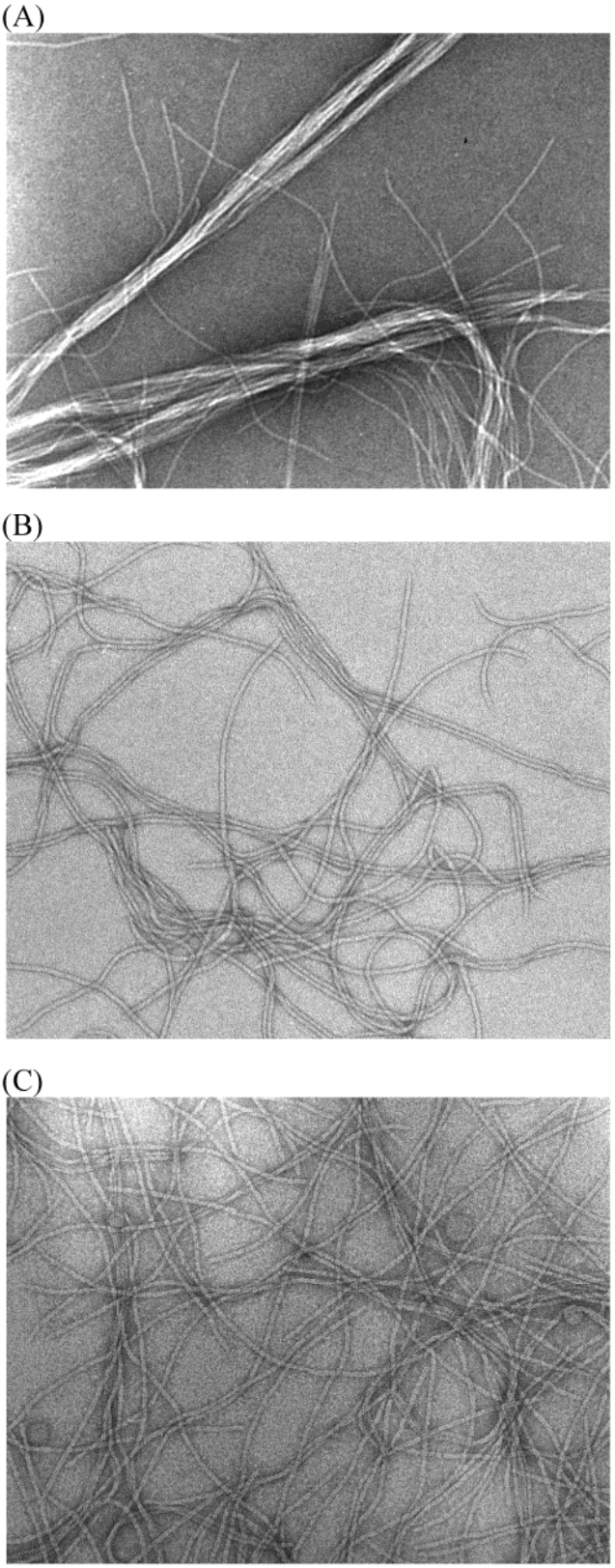

FIGURE 3: Representative electron micrographs of negatively stained (2% uranyl acetate) specimens of fd virus deposited on carbon-coated copper grids from solutions containing 17 μg/mL virus in 10 mM Tris and either no added NaCl (A), 50 mM NaCl (B), or 500 mM NaCl (C). Similar results were obtained in repeated trials over wide ranges of pH ($2 < pH < 11$).

ing of phage particles and accompanying cholesteric phase formation is anticipated. Therefore, the present attribution of Raman polarization effects to anisotropic orientation of virions in the concentrated phage solutions lacking NaCl is entirely consistent with previous findings. Further, the Raman evidence that disaggregation of filament clusters leads to isotropy of the virions in dilute phage solutions containing excess Na^+ is consistent with NMR dipolar coupling measurements (*30*).

The Raman polarization effects observed for low-salt solutions of the viruses are thus attributable to axial alignment of the virions. Such preferred virion alignment (with respect to the direction of polarization of the incident laser beam) may be regarded as localized cholesteric phase formation, which we have depicted schematically in Figure 2A. In general, a polarization effect is expected for every Raman band to which an anisotropic Raman tensor corresponds (*37*). At present, reliable Raman tensors are known for only a small number of vibrational modes of protein molecules, including the amide I mode of the peptide main chain and selective ring modes of Trp and Tyr side chains (*52*−*54*). A comparison of the results of Figure 1 with previously reported polarized Raman studies of oriented fd, Pf1, and Pf3 (*6*, *10*, *16*, *17*, *46*, *55*) indicates that the preferred direction of alignment in low-salt solutions is with the virion axis close to perpendicular to the axis of the sample capillary cell (Figure 2A). Random or isotropic distribution of filamentous virions in solutions containing a high salt/virus concentration ratio is depicted in Figure 2B.

Molecular Mechanism. Capsid surfaces of filamentous viruses are negatively charged, owing to the location of the relatively acidic N-terminal segment of the α-helical subunit on the capsid exterior. In the case of fd, for example, residues at or near the capsid surface include Glu 2, Asp 4, Asp 5, Lys 8, Asp 12, and Glu 20, which with the positively charged N terminus, yield a net charge of −3. Net negative charges also apply to the N-terminal segments of the coat subunits in Pf1 (−2), Pf3 (−1), and PH75 (−1). The phenomenon of lateral aggregation of anionic polyprotein assemblies, such as the filamentous viruses and F-actin filaments, has been compared with the phenomenon of DNA condensation (*33*, *51*) to which polyelectrolyte theory has been applied (*48*). The prevailing view is that such aggregative phenomena are driven by reduction of the axial charge density of the polyanion, which becomes increasingly favorable with decreasing salt concentrations. Conversely, filament disaggregation is driven by increasing salt concentrations, which increases the axial charge density. Thermodynamically, the balance between lateral aggregation and disaggregation depends on competition between salt−ion and salt−polyanion interactions. The precise molecular mechanism governing this phenomenon, however, remains unresolved.

Prospects. Figure 1 shows that many Raman bands of each filamentous virus are sensitive to salt-related virion alignment. A tabulation of the affected Raman bands is given in Table 1, which also lists the relative Raman band intensities, sign and magnitude of intensity change, and residue assignments. In cases where the nature of the normal mode of vibration is known, this information is also included. Importantly, the data of Table 1 constitute a catalog of protein Raman markers for which the respective Raman tensors *must* be anisotropic. Accordingly, these Raman markers are valuable targets for future Raman tensor determinations using techniques similar to those recently established for tryptophan-, tyrosine-, arginine-, and carboxylate-containing side chains (*53*, *54*, *56*, *57*).

The present results indicate that high- and low-salt concentrations favor minimal and optimal alignment, respectively, of filamentous viruses in solution. Accordingly, a high-salt concentration is recommended as an appropriate standard protocol for solution Raman studies of filamentous viruses. This would be particularly important for comparison of Raman spectral signatures of different viruses with one another. Conversely, a low-salt concentration is recommended for polarized Raman analyses, whether of flow-oriented solutions or mechanically drawn fibers.

Salt-dependent associative properties of the filamentous viruses may also be relevant to other experimental applications. For example, use of a filamentous virus solution as a medium to induce co-alignment of a dissolved protein for NMR solution structure determination would appear to be favored by low NaCl concentrations. On the other hand, high NaCl concentrations may be more appropriate for studies of substrate−ligand interactions by phage display technology.

ACKNOWLEDGMENT

This work was supported by NIH Grant GM50776.

REFERENCES

1. Webster, R. E. (1996) in *Phage Display of Peptides and Proteins* (Kay, B. K., Winter, J., and McCaffery, J., Eds.) pp 1−20, Academic Press, London, U.K.
2. Marvin, D. A. (1998) Filamentous phage structure, infection, and assembly, *Curr. Opin. Struct. Biol. 8*, 150−158.
3. Day, L. A., Marzec, C. J., Reisberg, S. A., and Casadevall, A. (1988) DNA packing in filamentous bacteriophages, *Annu. Rev. Biophys. Biophys. Chem. 17*, 509−539.
4. Pederson, D. M., Welsh, L. C., Marvin, D. A., Sampson, M., Perham, R. N., Yu, M., and Slater, M. R. (2001) The protein capsid of filamentous bacteriophage PH75 from *Thermus thermophilus*, *J. Mol. Biol. 309*, 401−421.
5. Marvin, D. A., Hale, R. D., Nave, C., and Citterich, M. H. (1994) Molecular models and structural comparisons of native and mutant class I filamentous bacteriophages: Ff (fd, f1, M13), If1, and IKe, *J. Mol. Biol. 235*, 260−286.
6. Overman, S. A., Tsuboi, M., and Thomas, G. J., Jr. (1996) Subunit orientation in the filamentous virus Ff (fd, f1, M13), *J. Mol. Biol. 259*, 331−336.
7. Takeuchi, H., Matsuno, M., Overman, S. A., and Thomas, G. J., Jr. (1996) Raman linear intensity difference of flow-oriented macromolecules: Orientation of the indole ring of tryptophan-26 in filamentous virus fd, *J. Am. Chem. Soc. 118*, 3498−3507.
8. Welsh, L. C., Symmons, M. F., Sturtevant, J. M., Marvin, D. A., and Perham, R. N. (1998) Structure of the capsid of Pf3 filamentous phage determined from X-ray fibre diffraction data at 3.1 Å resolution, *J. Mol. Biol. 283*, 155−177.
9. Welsh, L. C., Symmons, M. F., and Marvin, D. A. (2000) The molecular structure and structural transition of the α-helical capsid in filamentous bacteriophage Pf1, *Acta Crystallogr., Sect. D. 56* (Part 2), 137−150.
10. Tsuboi, M., Ushizawa, K., Nakamura, K., Benevides, J. M., Overman, S. A., and Thomas, G. J., Jr. (2001) Orientations of Tyr 21 and Tyr 24 in the capsid of filamentous virus Ff determined by polarized Raman spectroscopy, *Biochemistry 40*, 1238−1247.
11. Hunter, G. J., Rowitch, D. H., and Perham, R. N. (1987) Interactions between DNA and coat protein in the structure and assembly of filamentous bacteriophage fd, *Nature 327*, 252−254.
12. Deng, L. W., and Perham, R. N. (2002) Delineating the site of interaction on the pIII protein of filamentous bacteriophage fd with the F-pilus of *Escherichia coli*, *J. Mol. Biol. 319*, 603−614.

13. Haigh, N. G., and Webster, R. E. (1998) The major coat protein of filamentous bacteriophage f1 specifically pairs in the bacterial cytoplasmic membrane, *J. Mol. Biol. 279*, 19−29.
14. Haigh, N. G., and Webster, R. E. (1999) The pI and pXI assembly proteins serve separate and essential roles in filamentous phage assembly, *J. Mol. Biol. 293*, 1017−1027.
15. Blanch, E. W., Hecht, L., Syme, C. D., Volpetti, V., Lomonossoff, G. P., Nielsen, K., and Barron, L. D. (2002) Molecular structures of viruses from Raman optical activity, *J. Gen. Virol. 83*, 2593−2600.
16. Tsuboi, M., Overman, S. A., Nakamura, K., Rodriguez-Casado, A., and Thomas, G. J., Jr. (2003) Orientation and interactions of an essential tryptophan (Trp-38) in the capsid subunit of Pf3 filamentous virus, *Biophys. J. 84*, 1969−1976.
17. Tsuboi, M., Kubo, Y., Ikeda, T., Overman, S. A., Osman, O., and Thomas, G. J., Jr. (2003) Protein and DNA residue orientations in the filamentous virus Pf1 determined by polarized Raman and polarized FTIR spectroscopy, *Biochemistry 42*, 940−950.
18. Opalka, N., Beckmann, R., Boisset, N., Simon, M. N., Russel, M., and Darst, S. A. (2003) Structure of the filamentous phage pIV multimer by cryo-electron microscopy, *J. Mol. Biol. 325*, 461−470.
19. Nakamura, M., Tsumoto, K., Kumagai, I., and Ishimura, K. (2003) A morphologic study of filamentous phage infection of *Escherichia coli* using biotinylated phages, *FEBS Lett. 536*, 167−172.
20. Zeri, A. C., Mesleh, M. F., Nevzorov, A. A., and Opella, S. J. (2003) Structure of the coat protein in fd filamentous bacteriophage particles determined by solid-state NMR spectroscopy, *Proc. Natl. Acad. Sci. U.S.A. 100*, 6458−6463.
21. Davis, B. M., and Waldor, M. K. (2003) Filamentous phages linked to virulence of *Vibrio cholerae*, *Curr. Opin. Microbiol. 6*, 35−42.
22. Sambrook, J., and Russell, D. W. (2001) *Molecular Cloning: A Laboratory Manual*, Cold Spring Harbor Laboratory Press, Cold Spring Harbor, NY.
23. Azzazy, H. M., and Highsmith, W. E., Jr. (2002) Phage display technology: Clinical applications and recent innovations, *Clin. Biochem. 35*, 425−445.
24. Enshell-Seijffers, D., Denisov, D., Groisman, B., Smelyanski, L., Meyuhas, R., Gross, G., Denisova, G., and Gershoni, J. M. (2003) The mapping and reconstitution of a conformational discontinuous B-cell epitope of HIV-1, *J. Mol. Biol. 334*, 87−101.
25. Russel, M., Linderoth, N. A., and Sali, A. (1997) Filamentous phage assembly: Variation on a protein export theme, *Gene 192*, 23−32.
26. Roth, T. A., Weiss, G. A., Eigenbrot, C., and Sidhu, S. S. (2002) A minimized M13 coat protein defines the requirements for assembly into the bacteriophage particle, *J. Mol. Biol. 322*, 357−367.
27. Hansen, M. R., Hanson, P., and Pardi, A. (2000) Filamentous bacteriophage for aligning RNA, DNA, and proteins for measurement of nuclear magnetic resonance dipolar coupling interactions, *Methods Enzymol. 317*, 220−240.
28. Opella, S. J., Stewart, P. L., and Valentine, K. G. (1987) Protein structure by solid-state NMR spectroscopy, *Q. Rev. Biophys. 19*, 7−49.
29. Thomas, G. J., Jr., and Day, L. A. (1981) Conformational transitions in Pf3 and their implications for the structure and assembly of filamentous bacterial viruses, *Proc. Natl. Acad. Sci. U.S.A. 78*, 2962−2966.
30. Barrientos, L. G., Louis, J. M., and Gronenborn, A. M. (2001) Characterization of the cholesteric phase of filamentous bacteriophage fd for molecular alignment, *J. Magn. Reson. 149*, 154−158.
31. Thomas, G. J., Jr., Prescott, B., and Day, L. A. (1983) Structure similarity, difference, and variability in the filamentous viruses fd, If1, IKe, Pf1, Xf, and Pf3, *J. Mol. Biol. 165*, 321−356.
32. Day, L. A., Casadevall, A., Prescott, B., and Thomas, G. J., Jr. (1988) Raman spectroscopy of mercury(II) binding to two filamentous viruses: Ff (fd, M13, f1) and Pf1, *Biochemistry 27*, 706−711.
33. Tang, J. X., Janmey, P. A., Lyubartsev, A., and Nordenskiold, L. (2002) Metal ion-induced lateral aggregation of filamentous viruses fd and M13, *Biophys. J. 83*, 566−581.
34. Torbet, J., and Maret, G. (1979) Fibres of highly oriented Pf1 bacteriophage produced in a strong magnetic field, *J. Mol. Biol. 134*, 843−845.
35. Torbet, J., and Maret, G. (1981) High-field magnetic birefringence study of the structure of rodlike phages Pf1 and fd in solution, *Biopolymers 20*, 2657−2669.
36. Tuma, R., and Thomas, G. J., Jr. (2002) Applications in Life, Pharmaceutical, and Natural Sciences, in *Handbook of Vibrational Spectroscopy* (Chalmers, J. M., and Griffiths, P. R., Eds.) Vol. 5, pp 3519−353517, John Wiley and Sons, Chichester, U.K.
37. Tsuboi, M., and Thomas, G. J., Jr. (1997) Raman scattering tensors in biological molecules and their assemblies, *Appl. Spectrosc. Rev. 32*, 263−299.
38. Overman, S. A., and Thomas, G. J., Jr. (1995) Raman spectroscopy of the filamentous virus Ff (fd, fl, M13): Structural interpretation for coat protein aromatics, *Biochemistry 34*, 5440−5451.
39. Overman, S. A., and Thomas, G. J., Jr. (1998) Amide modes of the α-helix: Raman spectroscopy of filamentous virus fd containing peptide ^{13}C and ^{2}H labels in coat protein subunits, *Biochemistry 37*, 5654−5665.
40. Overman, S. A., and Thomas, G. J., Jr. (1999) Raman markers of nonaromatic side chains in an α-helix assembly: Ala, Asp, Glu, Gly, Ile, Leu, Lys, Ser, and Val residues of phage *fd* subunits, *Biochemistry 38*, 4018−4027.
41. Thomas, G. J., Jr. (2002) New structural insights from Raman spectroscopy of proteins and their assemblies, *Biopolymers 67*, 214−225.
42. Wen, Z. Q., Armstrong, A., and Thomas, G. J., Jr. (1999) Demonstration by ultraviolet resonance Raman spectroscopy of differences in DNA organization and interactions in filamentous viruses Pf1 and fd, *Biochemistry 38*, 3148−3156.
43. Wen, Z. Q., Overman, S. A., Bondre, P., and Thomas, G. J., Jr. (2001) Structure and organization of bacteriophage Pf3 probed by Raman and ultraviolet resonance Raman spectroscopy, *Biochemistry 40*, 449−458.
44. Thomas, G. J., Jr. and Barylski, J. (1970) Thermostating capillary cells for a laser-Raman spectrophotometer, *Appl. Spectrosc. 24*, 463−464.
45. Aubrey, K. L. and Thomas, G. J., Jr. (1991) Raman spectroscopy of filamentous bacteriophage Ff (fd, M13, f1) incorporating specifically deuterated alanine and tryptophan side chains: Assignments and structural interpretation, *Biophys. J. 61*, 1337−1349.
46. Tsuboi, M., Overman, S. A., and Thomas, G. J., Jr. (1996) Orientation of tryptophan-26 in coat protein subunits of the filamentous virus Ff by polarized Raman microspectroscopy, *Biochemistry 35*, 10403−10410.
47. Matsuno, M., Takeuchi, H., Overman, S. A., and Thomas, G. J., Jr. (1998) Orientations of tyrosines 21 and 24 in coat subunits of Ff filamentous virus: Determination by Raman linear intensity difference spectroscopy and implications for subunit packing, *Biophys. J. 74*, 3217−3225.
48. Record, M. T., Jr., Zhang, W., and Anderson, C. F. (1998) Analysis of effects of salts and uncharged solutes on protein and nucleic acid equilibria and processes: A practical guide to recognizing and interpreting polyelectrolyte effects, Hofmeister effects, and osmotic effects of salts, *Adv. Protein Chem. 51*, 281−353.
49. Tang, J. X., and Fraden, S. (1995) Isotropic-cholesteric phase transition in colloidal suspensions of filamentous bacteriophage fd, *Liq. Cryst. 19*, 459−467.
50. Tang, J. X., Ito, T., Tao, T., Traub, P., and Janmey, P. A. (1997) Opposite effects of electrostatics and steric exclusion on bundle formation by F-actin and other filamentous polyelectrolytes, *Biochemistry 36*, 12600−12607.
51. Tang, J. X., and Janmey, P. A. (1996) The polyelectrolyte nature of F-actin and the mechanism of actin bundle formation, *J. Biol. Chem. 271*, 8556−8563.
52. Tsuboi, M., Ikeda, T., and Ueda, T. (1991) Raman microscopy of a small unixial crystal: Tetragonal aspartame, *J. Raman Spectrosc. 22*, 619−626.
53. Tsuboi, M., Ueda, T., Ushizawa, K., Ezaki, Y., Overman, S. A., and Thomas, G. J., Jr. (1996) Raman tensors for the tryptophan side chain in proteins determined by polarized Raman microspectroscopy of oriented *N*-acetyl-L-tryptophan crystals, *J. Mol. Struct. 379*, 43−50.
54. Tsuboi, M., Ezaki, Y., Aida, M., Suzuki, M., Yimit, A., Ushizawa, K., and Ueda, T. (1998) Raman scattering tensors of tyrosine, *Biospectroscopy 4*, 61−71.
55. Tsuboi, M., Suzuki, M., Overman, S. A., and Thomas, G. J., Jr. (2000) Intensity of the polarized Raman band at 1340−1345 cm^{-1} as an indicator of protein α-helix orientation: Application to Pf1 filamentous virus, *Biochemistry 39*, 2677−2684.

56. Tsuboi, M., Aida, M., Nakamura, K., Bondre, P., Overman, S. A., Benevides, J. M., and Thomas, G. J., Jr. (2001) Raman tensors of arginine: A basis for determining orientations of arginine side chains in filamentous viruses (Pf1 and Pf3) by polarized Raman spectroscopy, *Biophys. J. 80*, 397a.
57. Tsuboi, M., Nakamura, K., Aida, M., Kubo, Y., Benevides, J. M., and Thomas, G. J., Jr. (2002) Raman tensor of the carboxylate anion: A basis for determining aspartate and glutamate side-chain orientations in proteins by polarized Raman spectroscopy, *Biophys. J. 82*, 457e.
58. Miura, T., and Thomas, G. J., Jr. (1995) Proteins: Structure, Function, and Engineering, in *Subcellular Biochemistry* (Biswas, B. B., and Roy, S., Eds.) Vol. 24, pp 55−99, Plenum Press, New York.

BI0485023